Effect of pH level and calcination on the production of calcium phosphates by acidic route of wet precipitation

J. G. Neves[1], D. Navarro da Rocha[2], C. C. Lopes[2], M. H. Prado da Silva[2], M. A. C. Sinhoreti[1], L. Correr-Sobrinho[1], M. A. A. Fraga[1], A. B. Correr[1]*

[1]*University of Campinas, Piracicaba Dental School, Department of Restorative Dentistry, Dental Materials Division, Piracicaba, SP, Brazil*

[2]*Military Institute of Engineering, Department of Mechanical and Materials Engineering, Rio de Janeiro, RJ, Brazil*

Abstract

Multiphasic calcium phosphate powders were synthesized by the acidic route, using lactic acid as a chelating agent that allows the production of a stable and rich solution of calcium and phosphate ions at room temperature. After pH adjusting, without varying the concentrations of precursor solution, XRD and FTIR analyses showed different CaP phases before and after heat treatment at 1000 °C. At pH 5, brushite plate-like particles were produced, while at higher pH levels (7 to 12) nano-hydroxyapatite particles were formed. After the calcination process, partial and total decomposition of hydroxyapatite in the β-TCP phase was explained by XRF analysis due to the calcium-deficient hydroxyapatite of synthesized samples at pH 7 and 10. This work presents an important method to synthesize any desired CaP phase compositions by varying the pH level and subsequently performing heat treatment, which has a direct effect on morphology, crystallinity, and formation of different CaP powders.

Keywords: brushite, calcium pyrophosphate, β-TCP, hydroxyapatite.

INTRODUCTION

The bone is a complex organic-inorganic composite structure. The organic phase is mainly composed of type I collagen, whereas the inorganic phase consists of non-stoichiometric hydroxyapatite (HA) crystals embedded between the collagen fibers. Crystallographic and chemical studies demonstrated that synthetic HA is similar to bone or enamel apatite *in vivo* [1]. Different synthesis methods of calcium phosphate (CaP) have been developed with diverse crystalline structures and morphology, as well as processed 3D scaffolds to stimulate bone ingrowth into adequate pores [2]. Moreover, CaP can be applied as a coating on titanium surface to enhance the osteoconductivity of a bioinert metallic implant [3]. Generally, biomaterials are classified according to the host tissue response. Bioinert materials do not stimulate bone formation but instead stimulate the formation of fibrous tissue, whereas bioactive materials directly bond with the bone and form a uniquely strong biomaterial-bone chemical interface [4]. Bone mineralization in presence of bioceramic is a multifactor and complex process that is regulated by several parameters, such as: chemical composition, physical structure (e.g. size and design of porosity, specific surface area, and topography), and degradation rate of graft material [5, 6]. Among bioactive ceramics, hydroxyapatite and tricalcium phosphate (TCP) are the most CaP investigated in the biomedical field. The mixture of HA and β-TCP is referred to as biphasic calcium phosphates (BCP). Bioactive behavior of BCP is associated with HA/β-TCP ratio: the lower the ratio, the higher the degradation. The application of a more soluble calcium phosphate phase, as β-TCP, is because of the limited *in vivo* reactivity of dense and stoichiometric HA [7]. Recently, the use of both brushite and monetite in the form of injectable cement and granules has been shown to be effective in vertical bone augmentation and bone defect repair [8, 9].

Over the last few years, several modifications on parameters such as calcium/phosphorus molar ratio, synthesis temperature, and reaction pH level have been investigated in order to obtain a distinct chemical characteristic of calcium phosphate ceramic [10]. Synthesis of biphasic and triphasic calcium phosphate have been developed in order to influence the degradation-bioactivity rate, which such behaviors are well-established in the literature as a direct effect [10]. However, a high degradation behavior is not accompanied by high bone repair due to distinct bone formation rate by host tissue; thereby it requires enough stable biomaterial to allow the bone formation. Therefore, the production of biphasic calcium phosphate is a potential material that can also be applied for large bone defect repair [11, 12]. The degradation process of the calcium phosphate surface causes a supersaturation of their ions, which leads to a precipitation process of carbonate-apatite. Hence, a release of controlled levels of calcium ions to allow an apatite formation is required for the success of the biomaterial. The control of calcium phosphate nanoparticles aims to optimize the mechanical properties and accelerate the healing process in bone defects with a synthetic material mimicking the natural apatite.

**nevesjoseguilherme@gmail.com*
https://orcid.org/0000-0003-1613-8496

Several preparation methods of HA powders have been utilized and can be classified into five groups: wet methods; dry methods; high-temperature processes; synthesis methods based on biogenic sources; and combination procedures [13]. The wet precipitation technique is the most popular and widely researched for HA synthesis, because of the relatively large amount of HA that can be produced at a reasonable cost [13, 14]. Another advantage of wet method precipitation for tissue engineering is due to the production of HA precipitates at room temperature with characteristics similar to mineral bone, instead of the HA synthesis at high temperatures that leads to the formation of a high and well-crystallized structure.

Among several methods to produce calcium phosphates, one of the most popular pairs of calcium and phosphate precursors employed is the $Ca(OH)_2/H_3PO_4$ [15]. However, it is worth mentioning that the solubility of calcium hydroxide in water is low, reducing the amount of calcium phosphate powder, as well as increasing the presence of unwanted secondary phases in the final product after room-temperature synthesis. As an alternative, by using lactic acid as a chelating agent, which is a carboxylic acid with one hydroxyl group attached to the α-position of the carboxyl group, the solubility of calcium mineral may be increased in the aqueous solution. In addition, the presence of calcium and lactate [$CH_3CH(OH)CO_2^-$] ions interacting with phosphoric acid leads to the formation of a stable and rich solution of calcium and phosphate ions at acidic pH level at room temperature. The pH adjusting of this calcium phosphate precursor solution may change both phase composition and the fraction of produced powder by precipitation, influencing the relative concentrations of the four polymorphs of phosphoric acid [16, 17]. The presence of specific $H_2PO_4^-$, HPO_4^{2-}, PO_4^{3-} anion is a predominant factor for the precipitation of a corresponding calcium phosphate phase. In particular, the desired phase composition of the calcium phosphate powders (prepared via acidic route without varying concentrations of precursors) is controlled by pH adjusting and later by the heat treatment of produced green powders.

In the present work, an acidic route of wet precipitation is presented as a simple two-step method, capable of producing single or multiphasic calcium phosphate powders, by controlling the pH level and subsequently calcining the produced green powders. This work aimed to investigate some parameters of the method described here and its influence on the phase composition of the produced calcium phosphates powders from an acidic solution, with a Ca/P molar ratio fixed at 1.67. It was hypothesized that the fixed concentration of calcium, lactate, and phosphate ions in the precursor solution does not interfere in the particle size, morphology, or phase composition after pH adjusting/heat treatment.

MATERIALS AND METHODS

Calcium phosphate synthesis: the acidic route of the wet precipitation method was performed in two steps. First, a precursor solution saturated in Ca^{2+} and PO_4^{3-} ions was prepared by mixing 1 mol/L lactic acid solution ($C_3H_6O_3$, Synth, CAS n° 79-33-4) to 0.5 mol/L calcium hydroxide solution [$Ca(OH)_2$, Merck, CAS n° 1305-62-0). Thus, 0.3 mol/L phosphoric acid (H_3PO_4, Merck, CAS n° 7664-38-2) was slowly added to the previously obtained solution [15]. All the materials were prepared by maintaining a Ca/P molar ratio fixed at 1.67, as in stoichiometric HA, at 25 °C. In the second step of the solution synthesis, the pH level and temperature were controlled by a bioreactor (BIO-TEC-PRO, Tecnal). The KOH solution was used to control the pH level at 5, 7, 10, and 12. The calcium phosphate precipitates were aged for 24 h and the solution was filtered under negative pressure in a vacuum pump system (Edwards). The filtered cake was resuspended in ultrapure water in order to remove the remaining KOH, up to neutralization pH. The filtrate was frozen at -27 °C (Hota 20FL, Analytical) for 48 h and dried in a freeze-dryer (Alpha 1-2 LDplus, Christ) at 4 mbar vacuum and -48 °C for 48 h. Then, the powders were deagglomerated and sieved through mesh size #150. The samples were heat-treated at 1000 °C for 1 h to evaluate the phase stability of calcium phosphate powders.

Characterization: the powders were characterized by X-ray diffraction (XRD) in a diffraction system (X'Pert MPD, Philips Panalytical) operating with CuKα radiation (λ=0.1540 nm) at 40 kV, 40 mA, a step of 0.02°, and 1 s/step from 10° to 80°. Fourier transform infrared spectroscopy (FTIR) analyses were performed using a spectrophotometer (Nicolet 6700, Thermo Sci.) with KBr transparent pellets, and the spectra were obtained in the 4000 to 400 cm^{-1} range, resolution of 4 cm^{-1}, and 32 scans. Scanning electron microscopy with energy dispersive spectroscopy (SEM-EDS) analyzes of the powders were performed in a microscope (Quanta 250 FEG, FEI) operating at both high and low vacuum modes between 1 and 30 kV. The powders were observed after Au deposition to avoid electron charging of the samples, maintaining the nanometric features. In addition, the direct measurement tool of microscope software enabled quick access to the measurement of particles in the nanometric or submicrometric scale. The mean particle size of the different calcium phosphate particles was obtained after five FEG-SEM images were acquired for each sample and, on average, seven particles were counted per image. For the synthesized samples at pH 7, both green and calcined powders, only submicrometer particles were measured. For elemental analysis, the calcium and phosphorus contents were determined semi-quantitatively by X-ray fluorescence spectroscopy (XRF, Axios, Malvern Panalytical) at 1 kW. The thermal behavior was analyzed by thermogravimetric analysis (TGA, TGA/DSC, Mettler) with nitrogen atmosphere, a flux of 100 mL/min, and heated twice to 1000 °C at 10 °C/min rate.

RESULTS AND DISCUSSION

Structural and chemical characterization: Fig. 1 shows the XRD patterns of the green powders investigated. In Fig. 1a, the presence of brushite (JCPDS 01-072-0713) as the

major phase and some peaks of hydroxyapatite (JCPDS 09-0432) were observed for synthesized samples at pH 5. The high crystallinity, as can be seen by the narrow width of the diffraction peak at half maximum intensity is characteristic for the brushite phase, when compared with the broad diffraction peaks of the hydroxyapatite phase (Fig. 1b) [17]. The fact that the synthesis was performed at an acidic pH level kinetically favored the brushite formation [18-20]. Otherwise, the main diffraction peaks of hydroxyapatite (JCPDS 09-0432) were observed in all other samples at physiological and high pH levels [20, 21], as shown in Fig. 1b. It was possible to note that the HA showed diffraction patterns compatible with nanometric crystallite size and/or low crystallinity, in accordance with the reported *in vivo* bone tissue when synthesized in physiological and higher pH level environments [17].

In addition to the pH level, the effect of processing temperature was examined and X-ray diffraction patterns of the produced calcium phosphates are shown in Fig. 2. The XRD patterns of all samples calcined at 1000 ºC showed a high crystallinity, as can be seen by the narrow and sharp diffraction peaks, similar to the highly mineralized dental tissue or single-crystalline skeletal elements [22]. In the present work, at the lowest pH level, the as-synthesized brushite was converted by heat treatment to calcium pyrophosphate (JCPDS 09-0346), and the hydroxyapatite was completely decomposed in the β-TCP phase (JCPDS 09-0169). Recent studies reported the use of calcium pyrophosphate and β-TCP for clinical use [23-25] as a potential alternative to pure hydroxyapatite. XRD patterns of calcined samples, previously synthesized under physiological conditions (pH 7), indicated a single β-TCP phase. The heat treatment of the sample synthesized at the pH level of 10 favored the partial formation of the hydroxyapatite phase, reaching a single calcium phosphate phase at pH 12. Thus, the null hypothesis was rejected.

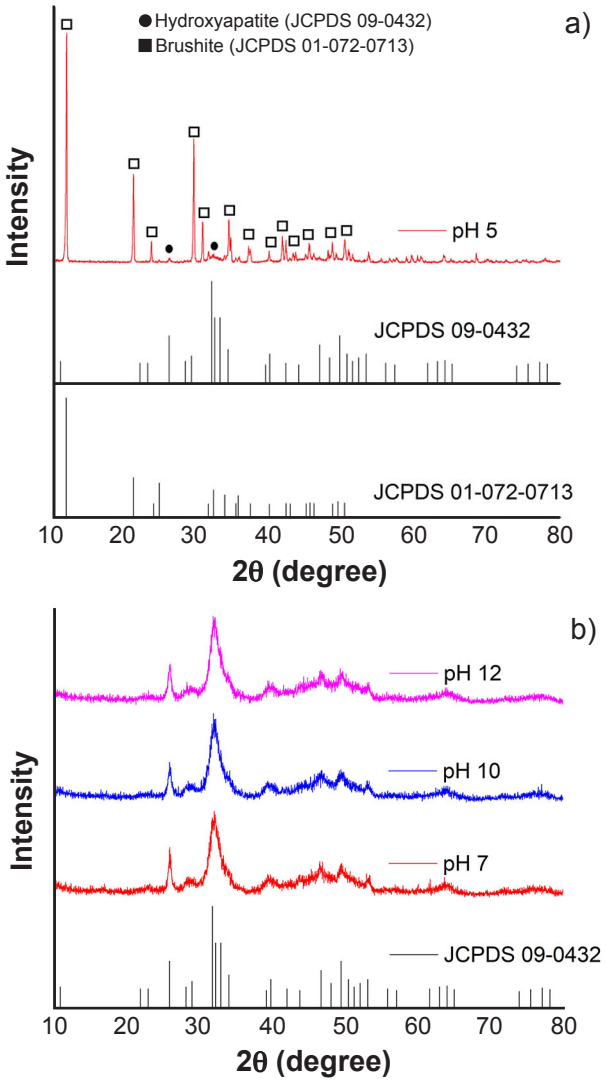

Figure 1: XRD patterns of synthesized green powders at pH 5 (a), and pH 7, 10, and 12 (b).

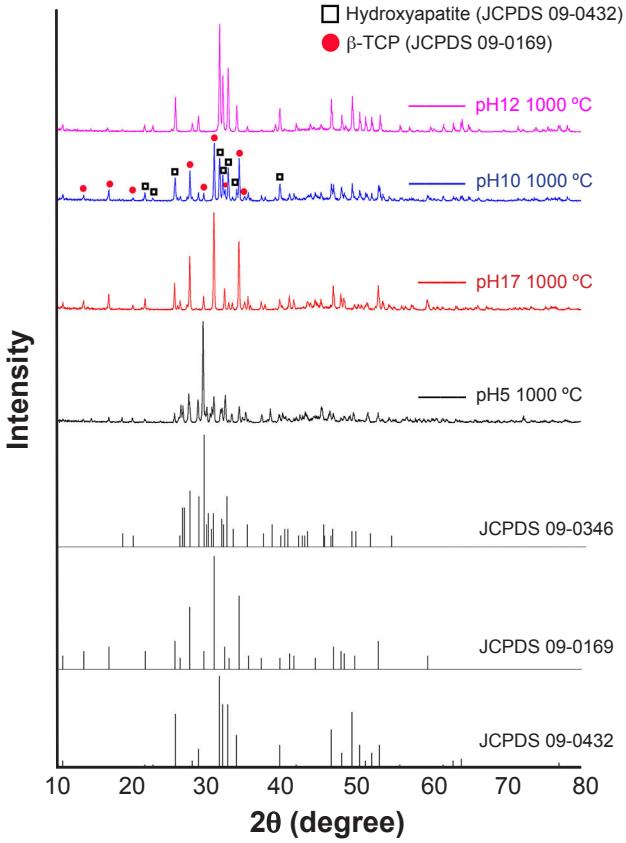

Figure 2: XRD patterns of calcined samples that were previously synthesized at pH 5 (single-phase calcium pyrophosphate), pH 7 (single-phase β-TCP), pH 10 (biphasic hydroxyapatite and β-TCP), and pH 12 (single-phase hydroxyapatite).

FTIR results: FTIR spectra of the calcium phosphates synthesized at different pH levels and, subsequently, submitted to calcination are shown in Figs. 3a and 3b, respectively. FTIR spectra showed characteristic bands of calcium phosphates represented by the functional phosphates (PO) and hydroxyl (OH). These results confirmed the presence of the calcium phosphate fingerprint patterns,

enabling the identification of brushite and hydroxyapatite phases in the different as-synthesized samples (Fig. 3a). The FTIR spectrum of the calcium phosphate sample synthesized at pH 5 (Fig. 3a) showed two doublets at 3500 and 3100 cm^{-1}, which corresponded to OH stretching bands at 3543, 3485, 3281, and 3163 cm^{-1} and the crystallization of brushite [26]. The presence of phosphate bands at 1208, 1134, 1065, and 987 cm^{-1} were observed. The absorbance band approximately at 1600 cm^{-1} was related to the water bending mode. The presence of an intense and sharp band was found at 875 cm^{-1}, which is specifically related to the P-O(H) stretching mode of the brushite mineral [27]. Phosphates groups were also detected at approximately 1000 cm^{-1}, which are bending mode peaks detected at 1221 and 874 cm^{-1} [28]. In addition to the phosphate and hydroxyl groups, the FTIR spectra of as-synthesized samples in physiological (pH=7) and higher pH levels showed the carbonate bands in the HA structure (Fig. 3a). The bands at 602, 563, and 575 cm^{-1} corresponded to the phosphate (PO_4^{3-}) ν_4 anti-symmetric deformation mode; the low-intensity band at 472 cm^{-1} was attributed to the PO_4^{3-} ν_2 symmetric deformation mode [27] and the infrared band at 970 cm^{-1} was due to the PO_4^{3-} ν_1 symmetrical stretching vibrational mode. The most intense bands of the FTIR spectrum were found in the region between 1097-950 cm^{-1} and corresponded to phosphate groups (PO_4^{3-}). Bands in the region between 1660-1300 and 870 cm^{-1} were found. This was an indication of the presence of carbonate apatite. This carbonate substitution probably occurred due to the absorption of carbon dioxide from the atmosphere [29].

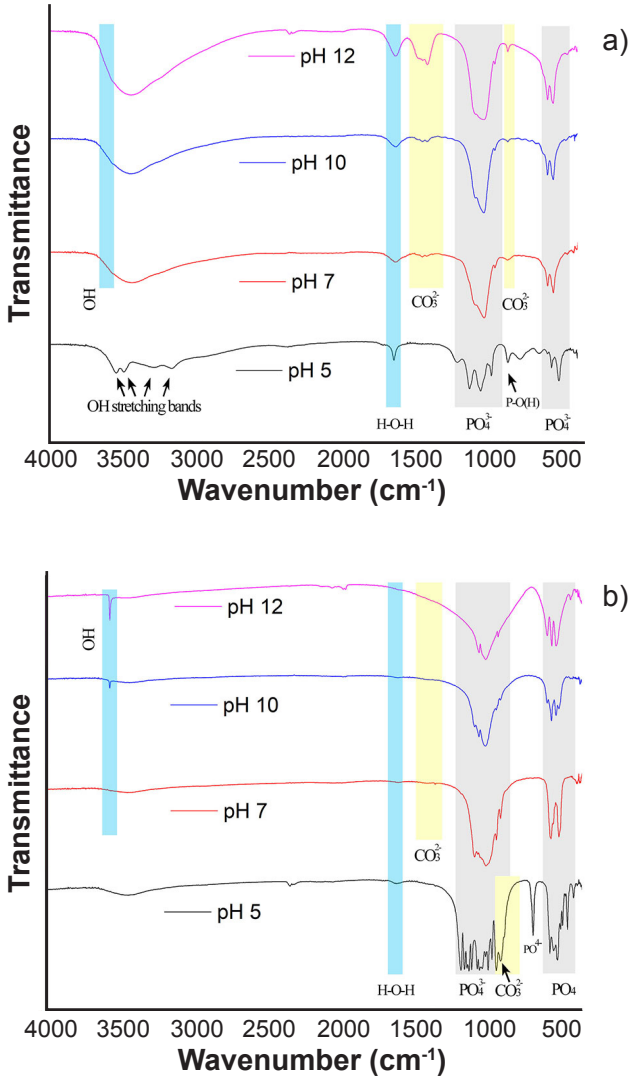

Figure 3: FTIR spectra of the calcium phosphate synthesized at different pH levels before (a) and after (b) calcination process.

FTIR spectra of calcined samples (Fig. 3b), previously synthesized above pH 7, showed a reduction of water band, between 3500-3000 cm^{-1}, in comparison with as-synthesized samples (Fig. 3a). Furthermore, the samples presented a decrease of hydroxyl band, characteristic of HA, according to the reduction of pH level in the synthesis. These results can be explained by the reduction of the hydroxyl groups (from water) by the calcination process and decomposition of the HA phase in a second phase, such as β-TCP and/or CaO [27]. As can be seen, the OH absorption band disappeared for the samples previously identified as single-phase β-TCP by XRD. The presence of β-TCP was observed from the band shoulders around 959, 975, and 1130 cm^{-1}, as well as changes in the positions of the PO_4^{3-} vibration bands indicating a partial or total decomposition of HA [30]. In addition, a triplet at approximately 630 cm^{-1} was related to the presence of the HA phase, which was not observed for β-TCP due to PO_4 group deformation, which was an effect of calcination [31]. However, even with heat treatment at 1000 ºC, the calcium pyrophosphate spectrum exhibited a broad band between 3600-2800 cm^{-1} and another weak band at 1600 cm^{-1} that corresponded to water OH vibration. The symmetric P-O stretching of PO_3^{2-} groups was verified due to the presence of 960, 1010, 1035, and 1120 cm^{-1} bands. The band at 885 cm^{-1} was attributed to the CO_3^{2-} asymmetric C-O stretching and the bands at 450, 480, 581, and 620 cm^{-1} were attributed to the PO_4^{2-} asymmetric O-P-O stretching. In addition, the presence of the PO^{4-} group at 725 cm^{-1} is characteristic of the calcium pyrophosphate phase [28].

FEG-SEM results: the morphology features and particle size of the calcium phosphate powders were controlled by changing the pH values of the synthesis (Fig. 4) and heat treatment (Fig. 5). At high pH, smaller size calcium phosphate nanoparticles were obtained compared to low pH values. In the Figs. 4b, 4c, and 4d, different sizes of nano-spherical and non-uniform hydroxyapatite aggregates can be observed in the synthesis at pH 7, 10, and 12, with mean particle sizes of 111±25, 86±16, and 48±6 nm, respectively. On the contrary, plate-like micrometric particle morphology from brushite was verified for pH 5 synthesis (Fig. 4a) with a particle size found in the 15-200 μm range and a mean particle size of 19±7 nm. Studies have shown that the degree of crystallinity and the decrease in phase impurity generation are directly influenced by the synthesis pH level [13, 32, 33]. Moreover, at low pH, there is the formation of macromolecules and this mechanism is explained by the fact that these molecules absorb the energy of the crystal formed

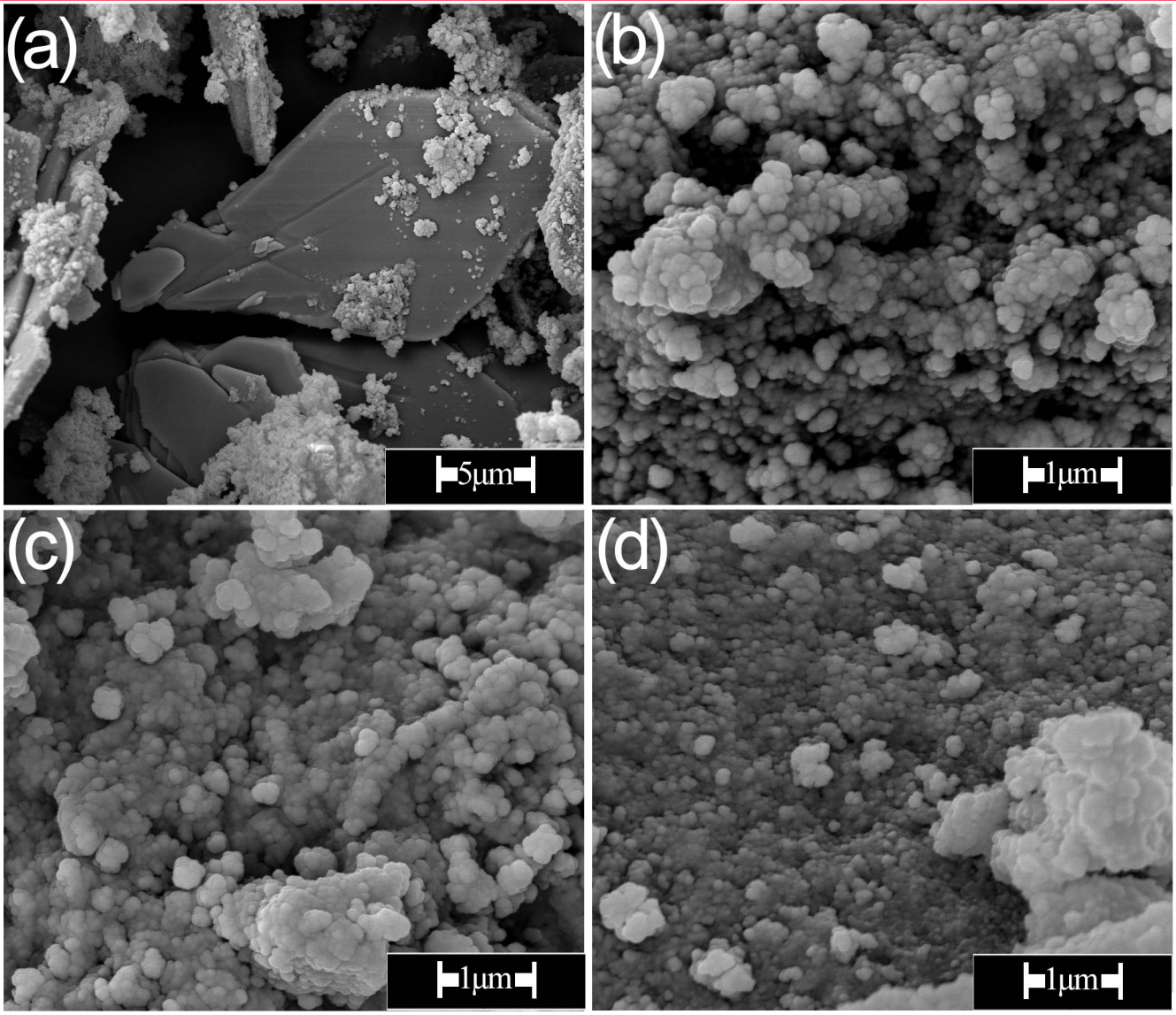

Figure 4: SEM micrographs of the samples synthesized at: a) pH 5; b) pH 7; c) pH 10; and d) pH 12.

in the reaction, generating particle growth [13, 32-34].

After the calcination process, for the group which was synthesized at pH 5 (Fig. 5a), the same macro- and micro-morphology were observed. However, the dense and smooth surface from plate-like brushite particles was modified to a porous surface, showing a mean particle size of 686±133 nm. Furthermore, it was observed a necking process and center approaching between particles, which were related to the growth of particles during the sintering process [13]. This process was due to the dynamic heating, where some particles may grow at the expense of their neighbors during sintering, resulting in an improvement of mechanical properties in some studies [35, 36]. For the calcined samples of previously synthesized samples at pH 7, 10, and 12 (Figs. 5b, 5c, and 5d), it was possible to observe the maintenance of the morphology of aggregates, however, the nano-size was increased to the submicron range after heat treatment, showing mean particle sizes of 761±70, 281±49, and 198±26 nm, respectively. In this context, the present work showed the importance of the synthesis of calcium phosphates via the acidic route of wet precipitation method in obtaining submicron and nanoparticles for biomaterials production, since the different particles sizes can improve the osteoblast function, speeding up the proliferation, adhesion, and differentiation, thus favoring the regeneration process [37, 38].

XRF results: XRF results (Table I) showed the presence of main chemical elements: calcium, phosphorus, and oxygen; some minor impurities (magnesium, potassium, and silicon) were also present. In this work, the highest Ca/P molar ratio (1.55) among all synthesis was observed for the sample synthesized at pH 12. The literature indicates that the Ca/P molar ratio of stoichiometric hydroxyapatite is 1.67; however, stable compositions were found in the range from 1.5 to 1.7, as can be seen in the XRD results in the present work (Fig. 1). It was also observed a decrease

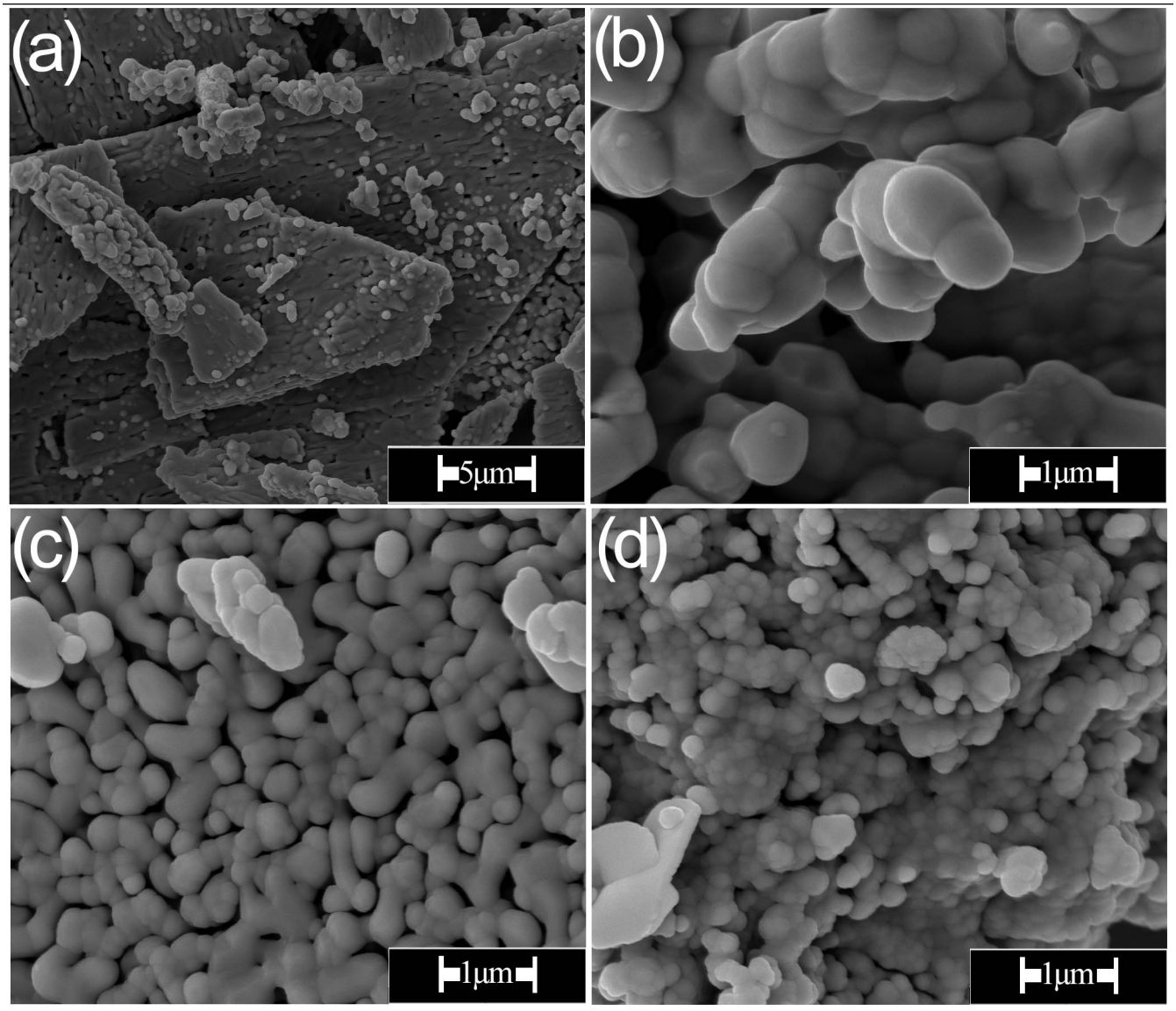

Figure 5: SEM micrographs of the samples synthesized at different pH levels after the calcination process: a) pH 5; b) pH 7; c) pH 10; and d) pH 12.

Table I - XRF results (%) of calcium phosphates synthesized at different pH levels.

pH	CaO	Ca	MCa	P_2O_5	P_2	MP	Ca/P
5	45.16	32.28	0.805	54.52	23.80	0.768	1.05
7	50.75	36.27	0.905	48.64	21.23	0.685	1.32
10	53.02	37.90	0.945	46.44	20.27	0.654	1.44
12	54.60	39.03	0.974	44.69	19.51	0.630	1.55

in the Ca/P molar ratio for synthesized samples at pH 10 (1.44), pH 7 (1.32), and pH 5 (1.05) [13, 39]. This result agreed with the poorly crystallized XRD diffraction patterns of these samples, which was directly related to the formation of calcium-deficient hydroxyapatite, and with the decomposition of HA to β-TCP after the calcination process. As expected, the acidic calcium phosphate phases verified by XRD and FTIR analysis, brushite and calcium pyrophosphate, were compatible with the lowest Ca/P ratio (1.05) found for the sample synthesized at pH 5.

Thermal behavior: the results of TGA of all calcium phosphate powders (pH 5, 7, 10, and 12) are shown in Fig. 6. The TGA curves showed a continuous weight loss in the range of 20 to 700 °C, where the first weight loss at low temperatures (<150 °C) was attributed to the removal of adsorbed water at the sample surfaces [40]. For the synthesized sample at pH 5 (Fig. 6a), the weight loss at 200 °C, around 15%, corresponded to water loss and the transformation of brushite (dicalcium phosphate dihydrate) in the monetite phase (dicalcium phosphate), as can be seen in the literature [41, 42]. The difference between the phases is the dihydrate structure of the brushite, as opposed

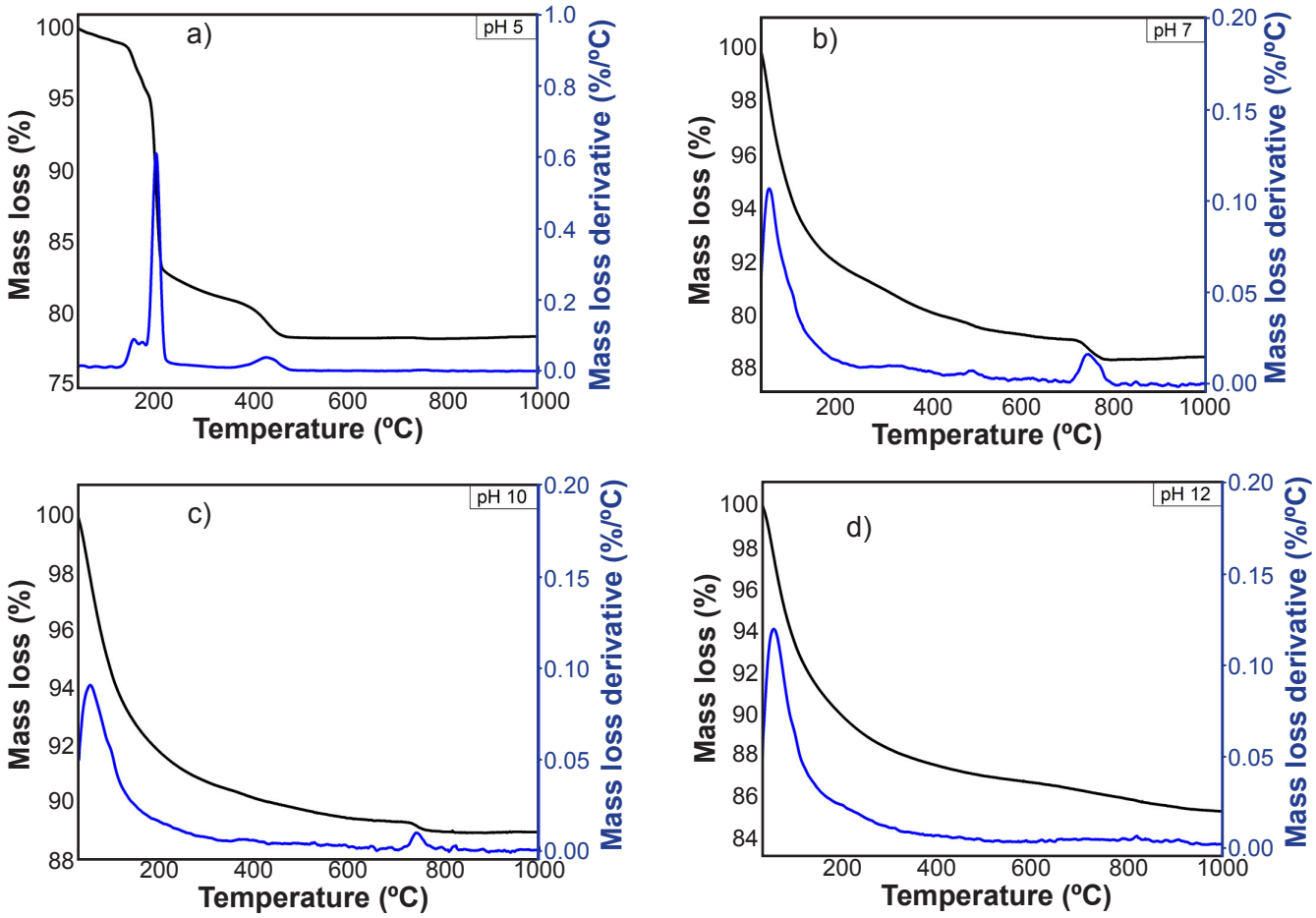

Figure 6: TGA (black line) and TGA's derivative (blue line) curves of the calcium phosphates at different pH levels: a) pH 5; b) pH 7; c) pH 10; and d) pH 12.

to the anhydrous structure of the monetite phase. In addition, the weight loss from 200 to 400 °C was around 20%, which can be explained by the decomposition of organic molecules and the transformation in the calcium pyrophosphate phase, confirmed by XRD in the present work (Fig. 2) [38, 43]. For the synthesized calcium phosphate powders at pH 7 and 10 (Figs. 6b and 6c), the weight loss of around 700 °C was related to the partial and total decomposition of hydroxyapatite, forming the β-TCP phase by a deoxygenation process, respectively [44]. These results are in accordance with the identification of a single β-TCP phase after the calcination process of the sample synthesized at pH 7, as well as for the produced biphasic sample at pH 10. However, the continuous weight loss from 20 to 1000 °C observed for the sample synthesized at pH 12 (Fig. 6d) is related to the crystallization process of hydroxyapatite and continuous water loss, as seen in the XRD and FTIR results [45-47]. This result demonstrated the high stability of the HA phase produced at pH 12, even after heat treatment at 1000 °C and Ca/P molar ratio of 1.55, below the stoichiometric HA [48]. Future biological testing is needed to address the possible differences between multiphase calcium phosphates, which may be more reactive within a regeneration process, as hydroxyapatite becomes even more crystalline after high-temperature treatment [41, 42].

CONCLUSIONS

The main conclusions of this work were: i) the use of lactic acid as a chelating agent played an essential role for the calcium phosphate synthesis via acidic route, responsible to produce a stable and rich solution of calcium and phosphate ions at room temperature; ii) it was possible to obtain single and multiphasic calcium phosphate powders, with a fixed Ca/P molar ratio at 1.67 in the acidic precursor solution, by the pH adjusting; and iii) after the calcination process of green powders, calcium pyrophosphate, β-TCP, and hydroxyapatite phases can be produced to achieve distinct morphology features and particle size.

ACKNOWLEDGEMENTS

The authors would like to acknowledge the institutions Analytical and Calibration Resources Laboratory (LRAC), Piracicaba Dental School - University of Campinas (FOP-UNICAMP), and R-Crio Stem Cells for their cooperation and support for the manuscript. The authors declare that they have no conflict of interest.

REFERENCES

[1] R.Z. LeGeros, Chem. Rev. **108**, 11 (2008) 4742.
[2] D.N. Rocha, L.R.O. Cruz, J.L. Prado Neto, N.M.E. Ayad, L.A. Gobbo, M.H.P. da Silva, Key Eng. Mater. **587**, 4 (2014) 128.
[3] D.N. da Rocha, L.R.O. Cruz, J.B. de Campos, J.L. dos Santos, R.L.S.B. Marçal, D.Q. Mijares, R.M. Barbosa, P.G. Coelho, M.H.P. da Silva, Ceram. Int. **45** (2019) 7568.
[4] V.R. Martinez-Zelaya, L. Zarranz, E.Z. Herrera, A.T. Alves, M.J. Uzeda, E. Mavropoulos, A.L. Rossi, A. Mello, J.M. Granjeiro, M.D. Calasans-Maia, A.M. Rossi, Int. J. Nanomedicine **14** (2019) 3471.
[5] N. Eliaz, N. Metoki, Materials **4** (2017) 334.
[6] M. Jamshaid Zafar, D. Zhu, Z. Zhang, Materials **20** (2019) 3361.
[7] Y. Deng, C. Jiang, C. Li, T. Li, M. Peng, J. Wang, K. Dai, Sci. Rep. **7** (2017) 5588.
[8] A. Laskus, A. Zgadzaj, J. Kolmas, Int. J. Mol. Sci. **12** (2018) 4042
[9] G. Cama, B. Gharibi, J.C. Knowles, S. Romeed, L. DiSilvio, S. Deb, J. R. Soc. Interface **11** (2014) 20140727.
[10] S.V. Dorozhkin, Acta Biomater. **8** (2012) 963.
[11] V. Klimecs, A. Grishulonoks, I. Salma, L. Neimane, J. Locs, E. Saurina, A. Skagers, J. Healthc. Eng. **2018** (2018) 4804902.
[12] G. Daculsi, A.P. Uzel, P. Weiss, E. Goyenvalle, E. Aguado, J. Mater. Sci. Mater. Med. **21** (2010) 855.
[13] M. Sadat-Shojai, M.T. Khorasani, E. Dinpanah-Khoshdargi, A. Jamshidi, Acta Biomater. **9** (2013) 7591.
[14] M.P. Ferraz, F.J. Monteiro, C.M. Manuel, J. Appl. Biomater. Biomech. **2** (2004) 74.
[15] A. Anwar, Q. Kanwal, S. Akbar, A. Munawar, A. Durrani, M.H. Farroq, Nanotechnol. Rev. **6**, 2 (2017) 149.
[16] S. Sun, Q. Chen, S. Sheth, G. Ran, Q. Song, ACS Sens. **5** (2020) 541.
[17] D.N. da Rocha, M.H.P. da Silva, J.B. de Campos, R.L.S.B. Marçal, D.Q. Mijares, P.G. Coelho, L.R.O. Cruz, J. Mater. Res. Technol. **7** (2018) 479.
[18] H.B. Pan, B.W. Darvell, Caries Res. **43** (2009) 254.
[19] A. Carino, C. Ludwig, A. Cervellino, E. Müller, A. Testino, Acta Biomater. **74** (2018) 478.
[20] K. Rubini, E. Boanini, A. Bigi, J. Funct. Biomater. **10** (2019) 1.
[21] C. Ruiz-Aguilar, U. Olivares-Pinto, E. Aguilar-Reyes, R. López-Juárez, I. Alfonso, Bol. Soc. Esp. Ceram. V. **5** (2018) 213.
[22] E. DiMasi, L.B. Gower (Eds.), "Characterization of biominerals and biomimetic materials", CRC Press (2017).
[23] J.H. Lee, B.S. Chang, U.O. Jeung, K.W. Park, M.S. Kim, C.K. Lee, Clin. Orthop. Surg. **3** (2011) 238.
[24] K.S. Lee, H.S. Han, Y.C. Kim, J.H. Lo Han, R.H. Seung, H.S. Lee, J.S. Chang, D.H. Lee, Mater. Res. Innov. **19** (2015) 86.
[25] A. Kakar, B.H.S. Rao, S. Hegde, N. Deshpande, A. Lindner, H. Nagursky, A. Patney, H. Mahajan, Int. J. Implant Dent. **3** (2017) 25.
[26] A. Hirsch, I. Azuri, L. Addadi, S. Weiner, K. Yang, S. Curtarolo, L. Kronik, Chem. Mater. **26** (2014) 2934.
[27] A. Slosarczyk, Z. Paszkiewicz, C. Paluszkiewicz, J. Mol. Struct. **744** (2005) 657.
[28] A.L. Daltin, S. Beaufils, T. Rouillon, P. Millet, J.P. Chopart, Ultrason. Sonochem. **58** (2019) 104662.
[29] R. Ghosh, R. Sarkar, Mater. Sci. Eng. **67** (2016) 345.
[30] M.L. Santos, A.O. Florentino, M.J. Saeki, A.H. Aparecida, M.V. Lia Fook, A.C. GuastaldiI, Eclet. Quím. **30** (2005) 29.
[31] J. Wang, L.L. Shaw, Adv. Mater. **19** (2007) 2364.
[32] Y. Cai, D. Mei, T. Jiang, J. Yao, Mater. Lett. **64** (2010) 2676.
[33] S. Catros, F. Guillemot, E. Lebraud, C. Chanseau, S. Perez, R. Bareille, J. Amédée, J.C. Fricain, IRBM **4**, 31 (2010) 226.
[34] G. Wei, J. Reichert, J. Bossert, K.D. Jandt, Biomacromolecules **9** (2008) 3258.
[35] E.S. Thian, N.H. Loh, K.A. Khor, S.B. Tor, Adv. Powder Technol. **12** (2001) 361.
[36] M.I. Ramli, A.B. Sulong, N. Muhamad, A. Muchtar, A. Arifin, F. Mohd Foudzi, M.S. Hammadi Al-Furjan, PLoS One **13** (2018) 206.
[37] P. Kubasiewicz-Ross, J. Hadzik, J. Seeliger, K. Kozak, K. Jurczyszyn, H. Gerber, M. Dominiak, C. Kunert-Keil, Ann. Anat. **213** (2017) 83.
[38] X. Gao, C. Dai, W. Liu, Y. Liu, R. Shen, X. Zheng, K. Duan, J. Weng, S. Qu, J. Mater. Sci. Mater. Med. **28** (2017) 83.
[39] K. Pluta, A. Sobczak-Kupiec, O. Półtorak, D. Malina, B. Tyliszczak, J. Biomed. Mater. Res. A **106** (2018) 1941.
[40] A.S. Khan, A.N. Hussain, L. Sidra, Z. Sarfraz, H. Khalid, M. Khan, F. Manzoor, L. Shahzadi, M. Yar, I.U. Rehman, Mater. Sci. Eng. C Mater. Biol. Appl. **80** (2017) 387.
[41] M.D. Vlad, S. Gómez, M. Barracó, J. López, E. Fernández, J. Mater. Sci. Mater. Med. **23** (2012) 2081.
[42] M.K. Boushell, N.T. Khanarian, R.Z. LeGeros, H.H. Lu, J. Biomed. Mater. Res. A **105** (2017) 2694.
[43] S.M.H. Dabiri, A. Lagazzo, B. Aliakbarian, M. Mehrjoo, E. Finocchio, L. Pastorino, J. Biomed. Mater. Res. A **107** (2019) 2063.
[44] J.L. Wang, Q. Chen, B.B. Du, L. Cao, H. Lin, Z.Y. Fan, J. Dong, Mater. Sci. Eng. C Mater. Biol. Appl. **1** (2018) 87.
[45] T. Wang, A. Dorner-Reisel, E. Muller, J. Eur. Ceram. Soc. **24** (2004) 693.
[46] R.L. Frost, S.J. Palme, Y. Xi, Spectrochim. Acta A Mol. Biomol. Spectrosc. **82** (2011) 132.
[47] K. Tonsuaadu, K.A. Gross, L. Pluduma, M.A. Veiderma, J. Therm. Anal. Calorim. **110** (2011) 647.
[48] S. Raynaud, E Champion, D. Bernache-Assollant, Biomaterials **4** (2002) 23.
(Rec. 03/04/2020, Rev. 02/07/2020, 21/10/2020, Ac. 28/12/2020)